nature communications

Article

https://doi.org/10.1038/s41467-024-54607-1

Membrane lipid homeostasis dually regulates conformational transition of phosphoethanolamine transferase EptA

Received: 14 March 2024

Accepted: 15 November 2024

Published online: 23 November 2024

Check for updates

Zhenyu Ma[1], Sue C. Nang[2], Zhuo Liu[1], Jingyi Zhu[3], Kaijie Mu[2], Limei Xu[3], Min Xiao[1], Lushan Wang[3], Jian Li[2] ✉ & Xukai Jiang[1] ✉

The phosphoethanolamine transferase EptA utilizes phosphatidylethanolamine (PE) in the bacterial cell membrane to modify the structure of lipopolysaccharide, thereby conferring antimicrobial resistance on Gram-negative pathogens. Previous studies have indicated that excessive consumption of PE can disrupt the cell membrane, leading to cell death. This implies the presence of a regulatory mechanism for EptA catalysis to maintain a balance between antimicrobial resistance and bacterial growth. Through microsecond-scale all-atom molecular dynamics simulations, we demonstrate that membrane lipid homeostasis modulates the conformational transition and catalytic activation of EptA. The conformation of EptA oscillates between closed and open states, ensuring the precise spatiotemporal sequence of substrates binding. Interestingly, the conformation of EptA is significantly influenced by its surrounding lipid microenvironment, particularly the PE proportion in the membrane. PE-rich membrane conditions initiate and stabilize the open conformation of EptA through both orthosteric and allosteric effects. Importantly, the reaction mediated by EptA gradually depletes PE in the membrane, ultimately hindering its conformational transition and catalytic activation. These findings collectively establish a self-promoted model, illustrating the regulatory mechanism of EptA during the development of antibiotic resistance.

The World Health Organization (WHO) and US Centers for Disease Control and Prevention (CDC) report that multidrug-resistant (MDR) Gram-negative bacteria, including *Acinetobacter baumannii*, *Pseudomonas aeruginosa*, and *Klebsiella pneumoniae*, have created a global drug resistance crisis that threatens modern medicine[1–3]. The outer membrane of Gram-negative bacteria is primarily comprised of lipopolysaccharides (LPS), phospholipids, and membrane proteins and functions as a crucial protective barrier that shields the bacteria from challenging external environments[4,5]. Catalyzed by different enzymes, cationic moieties such as phosphoethanolamine (pEtN), 4-amino-4-deoxy-L-arabinose, and galactosamine can be added to the lipid A or core components of LPS[6], augmenting the barrier properties of bacterial outer membrane and contributing to antibiotic resistance[4,7].

EptA is one of the most important LPS-modifying enzymes in Gram-negative bacteria[8]. Using phosphatidylethanolamine (PE) in bacterial cell membranes as a modifier group donor and Re LPS (i.e., lipid A with two 3-deoxy-D-manno-oct-2-ulosonic acid [KDO] sugars) as a modifier group acceptor, EptA mediates pEtN modification of LPS that leads to antimicrobial resistance[9]. Significantly, the protein encoded by the plasmid-borne *mcr-1* gene demonstrates substantial homology to EptA and facilitates identical LPS modifications[10,11]. The horizontal gene transfer capability of the *mcr-1* gene among diverse

[1]National Glycoengineering Research Center, Shandong University, Qingdao, China. [2]Biomedicine Discovery Institute, Monash University, Melbourne, Australia. [3]State Key Laboratory of Microbial Technology, Shandong University, Qingdao, China. ✉e-mail: jian.li@monash.edu; xukai.jiang@sdu.edu.cn

bacteria significantly amplifies the deleterious impact of LPS pEtN modification, intensifying bacterial resistance[12,13].

EptA contains an N-terminal transmembrane domain and a C-terminal soluble domain, with the active center for enzymatic catalysis situated between the two domains (Fig. 1a)[14]. Previous studies have elucidated that EptA catalysis follows a "ping-pong mechanism" involving sequential binding to two substrates, PE and Re LPS[15]. Interestingly, recent experiments have shown that overexpression of MCR-1 (an EptA homology) can induce cell membrane damage and bacterial death, presumably due to excessive consumption of PE in the cell membrane[16]. In addition, in Gram-negative bacteria with antibiotic resistance mediated by LPS modification, the proportion of pEtN-modified LPS in the outer membrane is strictly controlled[17]. Such data suggest that catalysis by EptA is strictly regulated by bacteria, although current research on its regulatory mechanism remains notably limited.

Structural biology investigations have revealed that the catalytically active center situated between the transmembrane and soluble domains of EptA lacks the capacity to accommodate the Re LPS molecule. This finding suggests a substantial conformational transition in EptA occurs during catalysis, leading to the formation of a larger substrate binding pocket. Anandhi Anandan et al. empirically verified the existence of distinct conformational states of EptA, demonstrating through molecular dynamics (MD) simulations that it can adopt an open conformation, which diverges from the closed conformation observed in crystalline structures[14]. In this open conformation, the substrate binding pocket undergoes a significant expansion, which is essential for Re LPS binding and completion of the catalytic process[14,18]. These investigations highlight the intricate conformational dynamics of EptA, contributing valuable insights into the interplay between protein conformation and catalytic function. However, the regulatory mechanisms governing the conformational transition of EptA within the cellular membrane environment remain elusive.

Herein, we demonstrate that EptA conformational transition and catalytic activation are regulated by the lipid homeostasis of the cell membrane. Employing microsecond-scale all-atom MD simulations, we reconstructed the dynamic cycling process from closed conformation to open conformation experienced during EptA catalysis. Our findings demonstrate that PE and Re LPS enter the substrate binding pocket of EptA through different access pathways. Combining these results with virtual mutations and evolutionary dynamics analysis, we establish that the interaction at the EptA domain interface is dynamic and governed by the binding of the PE substrate. Crucially, the interaction of the soluble domain with the membrane emerges as a key factor in maintaining the open conformation. Simultaneously, alterations in the local lipid environment resulting from EptA catalysis impact the interaction between EptA and the cell membrane, thereby

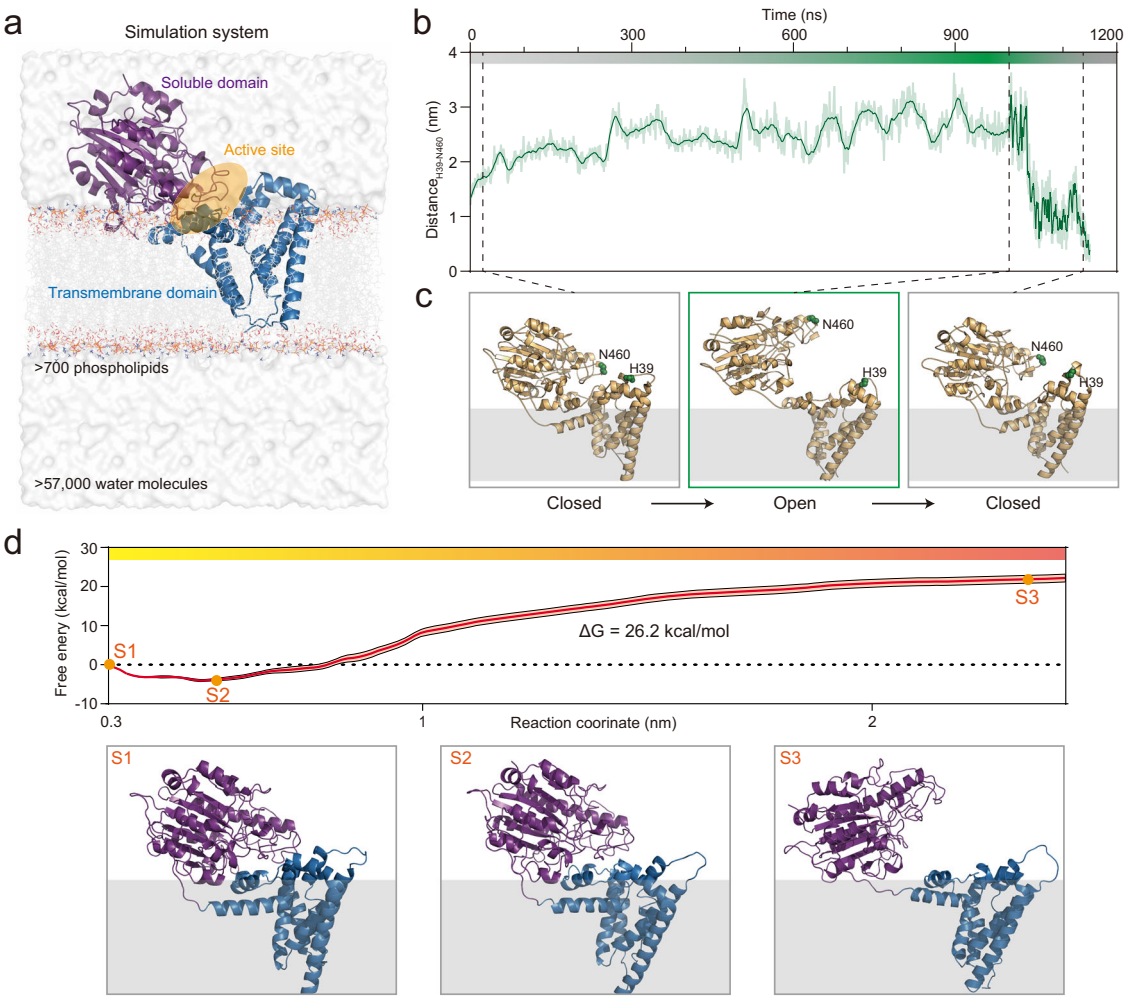

Fig. 1 | Conformational transition of EptA. a Simulation system for EptA in a bacterial cell membrane. The transmembrane and soluble domains are coloured blue and purple, respectively. The enzymatic active center is labelled. **b** The distances between H39 and N460 are calculated to indicate the process of the conformational transition of EptA. Source data are provided as a Source Data file. **c** Representative snapshots of EptA conformations in the membrane condition. The locations of H39 and N460 used for the distance calculations are labelled. **d** Free energy profile for the conformational transition process of EptA, along with representative structural snapshots (n = 100 independent estimations; data are presented as mean values ± SD). Source data are provided as a Source Data file.

regulating the transition between the two conformations. From a protein-lipid interaction perspective, these findings inform a 'self-promoted model' to explain the catalytic regulation of EptA and provide insights into the intricate balance between bacterial resistance and bacterial survival.

Results

Conformational transition of EptA creates distinct entry paths for PE and Re LPS

In the crystal structure (PDB ID: 5FGN), the transmembrane and soluble domains of EptA are in proximity, presenting a closed conformation[14]. To explore potential conformational transition processes of EptA, we employed the structure deposited in Protein Data Bank to establish an all-atom MD simulation system for EptA within the bacterial cell membrane model composed of 1,2-dipalmitoyl-sn-glycero-3-phosphoethanolamine (DPPE) (Fig. 1a)[14]. We observed that the EptA soluble domain gradually separated from the transmembrane domain, adopting an open conformation around 250 ns (Movie S1), which persisted until 1 microsecond (Fig. 1b). During this transition, the distance between the H39 residue (transmembrane domain) and the N460 residue (soluble domain) gradually increased from 1.3 nm to ~3 nm (Fig. 1b, c). Interestingly, when we took the last-frame structure of EptA (in open conformation) and placed it in a membrane composed of phosphatidylglycerol (PG), EptA quickly transitioned to a closed conformation after ~80 ns of simulation (Movie S2), with the distance between H39 and N460 gradually decreasing from 3 nm to ~1 nm (Fig. 1b, c). These results underscore the close correlation between the conformation of EptA and the lipid environment of the cell membrane in which it is situated.

To further investigate the thermodynamics governing the conformational transition of EptA, we employed the umbrella sampling approach to analyze the free energy profile of the transition process (Figs. 1d and S1). The results revealed that the overall free energy barrier was approximately 26.2 kcal/mol for the transition from the closed state in the crystal structure to the open state. Notably, the free energy barrier primarily resulted from the disruption of interactions between the transmembrane and soluble domains of EptA, implying the critical role of the hinge region in modulating its conformational transition.

The catalytically active center of EptA is located between its transmembrane and soluble domains. Upon the formation of the open conformation, the internal volume of the active center increases significantly (Fig. 1c). This observed conformational change is postulated to facilitate precise binding to PE and Re LPS—two substrates with differing molecular sizes[14]. To investigate the binding process of EptA to PE and Re LPS, we observed the spontaneous binding process of PE to EptA in its closed conformation and Re LPS to EptA in its open conformation within the cell membrane environment. When EptA was in the closed conformation, PE molecules located in the cell membrane were able to spontaneously rise and cross a channel composed of PH2-PH2' helices (Fig. 2a), eventually forming stable interactions with the substrate binding pocket. At this time, the hydrophilic head of PE primarily bound to surrounding amino acid residues of EptA, such as E114, T280, D324, and H383, while its hydrophobic carbon chain interacted with the amino acid residues N106, V107, T110, and L118 (Fig. 2b), consistent with previous results[19]. Importantly, it should be noted that Re LPS is larger than PE, and that the PH2-PH2' helices do not provide sufficient space for the passage of Re LPS. In our simulations, we observed that Re LPS molecules spontaneously approached the expanded substrate binding pocket within the open conformation of EptA through radial flow within the membrane. Despite this proximity, Re LPS molecules did not fully enter the binding pocket and did not traverse the channel formed by the PH2-PH2' helices (Fig. 2c). At this time, the hydrophilic head of Re LPS bound to the surrounding amino acid residues Q109, K203, W207, K208, and E302, while its hydrophobic carbon chain remained in the cell membrane environment bound to the surrounding amino acid residues L108, Y204, N211, and P213 (Fig. 2d).

We further calculated the interaction energies of PE and Re LPS with EptA at the amino acid residue level. E114 and D324 were the main contributors to PE binding, while Q109 and W207 were the main contributors to Re LPS binding (Fig. 2e). Notably, there were substantial differences in the key functional amino acid residues involved in the binding of PE and Re LPS. These results suggest that the conformational transition of EptA creates distinct entry pathways and binding modes for the two substrates, thereby enabling the precise spatiotemporal sequence of their binding.

Binding of PE promotes the conformational transition of EptA by altering the interfacial interaction between domains

The aforementioned analysis establishes that the conformational transition of EptA is likely essential for its proper engagement with distinct substrates to complete catalysis. This raises the question: How is the conformational transition of EptA achieved? Our initial focus was on the interfacial interactions between the EptA transmembrane and soluble domains, as the dynamic switching motion between these domains is a characteristic feature of the conformational transition (Fig. 3a). Structural examination revealed several electrostatic interaction pairs between the EptA transmembrane and soluble domains in the closed conformation, including R117-E389, R117-E352, E114-K328, and R209-D297. However, these electrostatic interaction pairs are entirely absent in the open conformation (Fig. 3b). To explore the relationship between these interfacial interactions and the EptA conformational transition, we calculated the evolution of each interaction pair throughout the simulations. These electrostatic interactions progressively weakened and ultimately disappeared after 150 ns (Fig. 3c), corresponding to the time when EptA began transitioning from the closed to the open conformation.

A significant observation was that the disappearance of the aforementioned electrostatic interaction pairs was closely linked to substrate binding, specifically to PE. Upon binding of PE to EptA, its pEtN group formed hydrogen bonds with E114 and K328, thereby preventing the formation of electrostatic interactions between these two residues (Figs. 3d and S2). This alteration in interactions may facilitate the opening of the hinge region between the EptA transmembrane and soluble domains. Due to limitations in molecular simulation sampling, only some systems exhibited spontaneous binding of PE molecules to the active center of EptA. Interestingly, we observed that the formation of the EptA open conformation occurred concurrently with PE binding. Conversely, the transition of EptA from a closed to an open conformation was not observed in a system lacking PE binding (Fig. 3e). We also calculated the free energies governing the conformational transition of *Nm*EptA in PE bound and unbound states. The results showed that PE binding significantly decreased the free energy barrier by approximately 21.9 kcal/mol, further indicating the role of PE binding in promoting the conformational transition of EptA (Fig. S3). These findings suggest that PE binding competitively disrupts the interactions between the transmembrane and soluble domains of EptA, thereby creating favorable conditions for its conformational transition.

The cell membrane lipid nano-environment regulates the stability of the EptA open conformation

During the transition from a closed to an open conformation, EptA exhibits a movement where its soluble domain progressively distances itself from the transmembrane domain and gradually approaches the cell membrane surface (Fig. 4a). Surface potential analysis of the EptA soluble domain revealed a substantial number of acidic residues on the dorsal region, including D292, D297, E298, D309, E317, E322, D324, D338, E346, D370, D372, and E533 (Figs. 4a and S4). These residues

https://doi.org/10.1038/s41467-024-54607-1

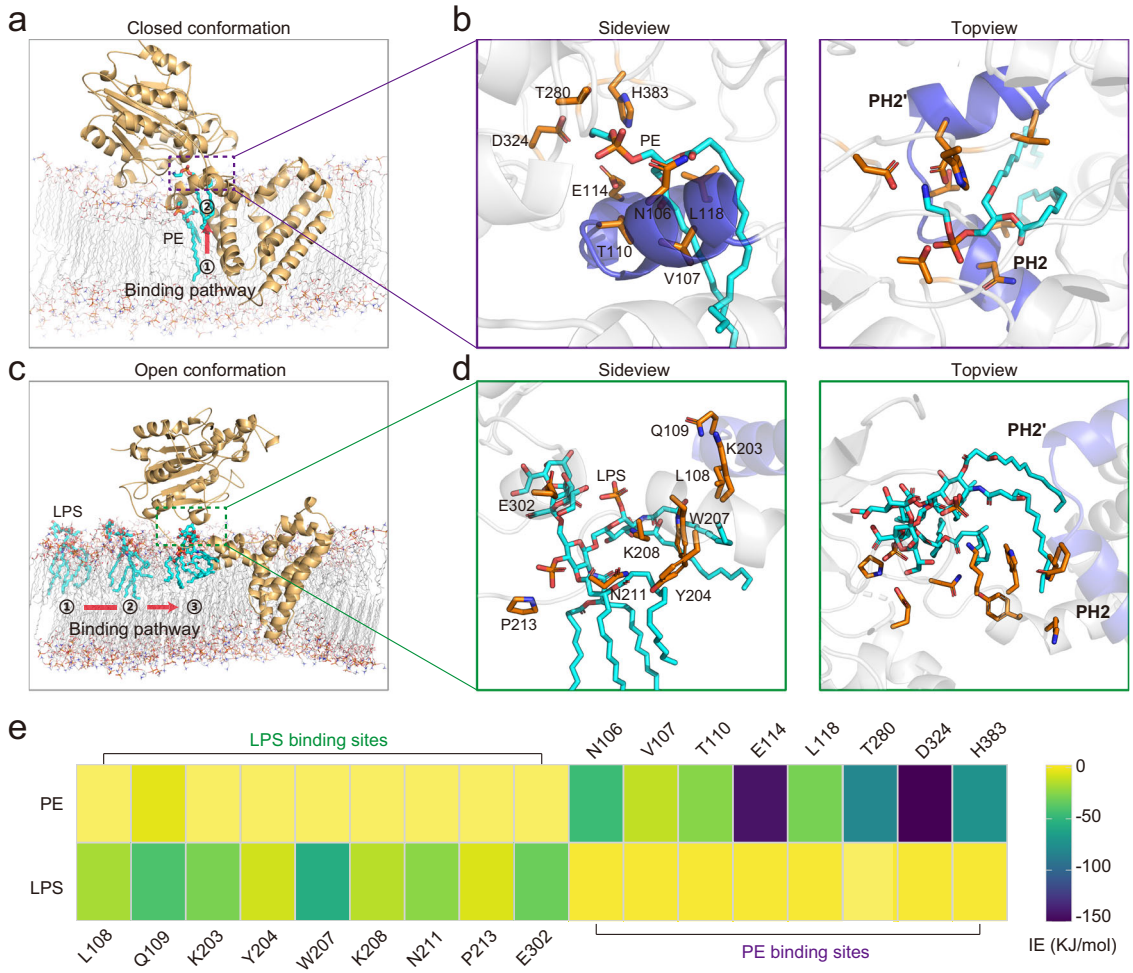

Fig. 2 | Conformational transition of EptA creates distinct entry pathways for PE and LPS. a Entry pathway for PE to access the active center of EptA in its closed conformation. **b** Interaction network between PE and the active site residues (orange sticks) of EptA. The PH2 and PH2′ helices are highlighted in blue. **c** Entry pathway for Re LPS to access the active center of EptA in its open conformation. **d** Interaction network between Re LPS and the active site residues (orange sticks) of EptA. The PH2 and PH2′ helices are highlighted in blue. **e** Cluster analysis of the interaction energy (IE) between EptA and PE, and between EptA and Re LPS. Data are shown as means. The color spectrum from yellow to purple indicates the increase in the intensity of IE. Source data are provided as a Source Data file.

create numerous regions of negative potential on the protein surface of the EptA soluble domain in proximity to the cell membrane (Fig. 4b). Notably, these acidic residues progressively approach the cell membrane surface during the opening of the EptA conformation (Fig. 4a) and establish stable interactions with PE molecules in the cell membrane (Fig. 4c). We speculate that these interactions play a crucial role in stabilizing the open conformation of EptA. An evolutionary analysis of 7308 EptA protein sequences from various bacteria revealed a high degree of conservation in these acidic residues during the molecular evolution of EptA (Fig. 4d). From an evolutionary perspective, this observation further suggests that these residues may be of significant importance to the biological function of EptA.

To further explore the contribution of these acidic residues in maintaining the open conformation of EptA, we specifically targeted three residues—D309, E317, and D370—which are located in the central β-fold layer and the α-helix layers on either side of the EptA soluble domain for computational mutational analysis (Fig. 4e). We designed single-site mutants D309A, E317A, and D370A; double-sites mutants D309A/E317A, D309A/D370A, and E317A/D370A; and the triple-site mutant D309A/E317A/D370A. We assessed the effect of these mutations on the stability of open conformation by calculating the distances between the residues H39 and N460 (Fig. 4f). A distance cutoff of 2 nm was used to define the formation of the closed conformation of EptA. Based on conformation sampling from three simulation replicates, the probability of forming the closed conformation was less than 5% for all single-site mutants and the double-sites mutants D309A/E317A and E317A/D370A. In contrast, the probability increased significantly to 26.61% and 32.27% for the mutants D309A/D370A and D309A/E317A/D370A, respectively. These results indicate that the acidic residues likely play a key role in maintaining the open conformation of EptA.

In the EptA-catalyzed reaction, PE molecules in the cell membrane serve as the donors of the LPS modification group and are continuously consumed as the reaction progresses. To explore the potential impact of this consumption on interactions with acidic amino acid residues in the soluble domain, we designed a series of cell membrane models in which the molar content of PE was gradually reduced from 100% to 0%. We observed the conformational dynamics of EptA in these varying environments, with all systems initialized in the open conformation. As the PE content decreased, there was an acceleration in the transition of EptA from an open to a closed conformation—in other words, a gradual reduction in the time maintained in the open conformation (Fig. 5). Specifically, EptA could sustain an open conformation in cell membranes with 100% and 80% PE content. In the cell membrane with 60% PE content, EptA began transitioning to a closed conformation after approximately 373 ns of simulation.

https://doi.org/10.1038/s41467-024-54607-1

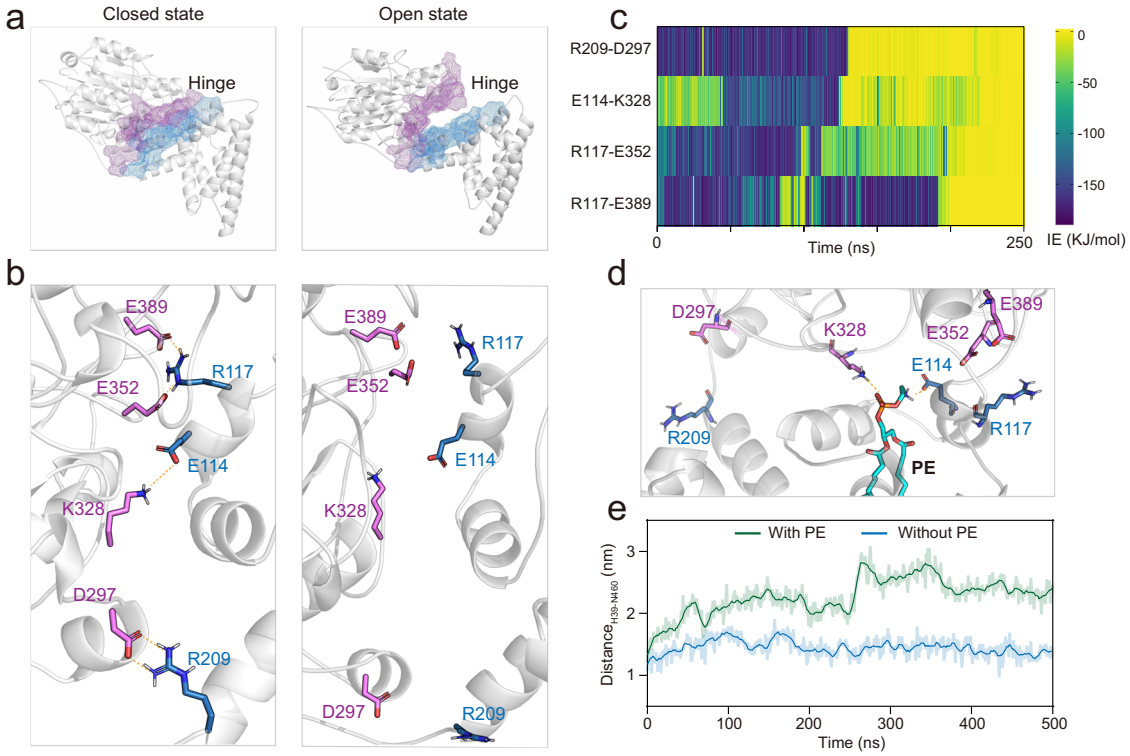

Fig. 3 | Interfacial interaction of EptA changes upon binding to PE. a The hinge region of EptA exhibits distinct morphologies in the closed and open conformations. The contact residues are shown in a mesh model, with the transmembrane and soluble domains presented in blue and purple, respectively. **b** Electrostatic interactions between the transmembrane and soluble domains vary across different conformations of EptA. The interactions are shown as dashed lines. **c** Evolution of the electrostatic interaction during the simulations of EptA opening. Source data are provided as a Source Data file. **d** Interactions between bound PE and interfacial residues. The hydrogen bonds are shown in dashed lines. **e** The distances between H39 and N460 in both the pure EptA system and the EptA-PE complex system during the simulations. Source data are provided as a Source Data file.

Closure was initiated after 128 ns in the cell membrane with 40% PE content, after 117 ns in the cell membrane with 20% PE content, and after 69 ns in the cell membrane with 0% PE content. Additionally, similar dynamic behaviors were observed in the simulation replicates (Table S1 and Fig. S5). These findings indicate that variations in PE content within cell membranes may alter the strength of interaction between cell membranes and acidic amino acid residues in the soluble domain, thereby influencing the conformational transition of EptA. Importantly, change in PE content in the cell membrane environment where EptA is situated are a direct consequence of its mediated catalytic reaction, as PE is one of the essential substrates for the EptA catalytic process.

Functional mutagenesis validates the roles of key residues on the hinge and dorsal regions of EptA

To validate the roles of key residues identified in EptA, we employed the plasmid-borne *mcr-1* gene as a template for a functional mutagenesis study. The pEtN transferase (i.e., MCR-1) encoded by the *mcr-1* gene is structurally similar to EptA (Fig. S6) and catalyzes the same pEtN modifications of LPS. Consistent with EptA, several electrostatic interaction pairs are present in the hinge region of MCR-1 (K212-D302/D304 and D119-K401/R402), and there are many acidic residues on the dorsal region of its soluble domain (D314, D317, D331, D337, D374, and D375) (Fig. 6a). Based on the simulation analysis of EptA, we hypothesized that these residues may also play critical roles in modulating the conformational transition and catalytic activity of MCR-1.

To test this hypothesis, we design a series of mutations at these positions and examined their effects on the catalytic activity of MCR-1 by measuring the minimum inhibitory concentrations (MIC) of colistin against *Escherichia. coli* strains expressing different MCR-1 mutants (Fig. 6b). The MICs were below 0.125 mg/L for strains *E. coli* DH5α and *E. coli* DH5α-pUC19, while the MIC was 4 mg/L for *E. coli* DH5α-pUC19*mcr-1*. The MIC was 4 mg/L for the strain expressing the MCR-1 mutant D302A/D304A; notably, the MIC was less than 0.125 mg/L against the strain expressing the mutant K401A/R402A. The MIC of the combination mutant D302A/D304A/K401A/R402A was also significantly decreased to 0.25 mg/L. These results indicate that K401 and R402 in the hinge region play a key role in the catalysis of MCR-1. Notably, mutations of the acidic residues in the dorsal region of the MCR-1 soluble domain exhibited a "dose-dependent" effect on protein activity. The single-site mutation D314A and double-site mutation D314A/D317A did not affect the activity of MCR-1, while the triple-site mutation D314A/D317A/D331A and quadruple-site mutation D314A/D317A/D331A/D337A slightly reduced MCR-1 activity. Importantly, the quintuple-site mutation D314A/D317A/D331A/D337A/D374A and sextuple-site mutation D314A/D317A/D331A/D337A/D374A/D375A significantly attenuated the MCR-1 activity. These in vitro results with MCR-1 were consistent with the simulation predictions for EptA, and further demonstrated that the electrostatic residues in the hinge region and the acidic residues in the dorsal region of the soluble domain are important for the catalytic activity of pEtN transferase.

EptA from various bacterial sources demonstrate a consistent conformational regulatory mechanism

To explore the universality of the conformational regulation mechanism of EptA, we conducted an evolutionary analysis on the sequences of EptA from 160 bacterial species. Based on their evolutionary relationships, they were categorized into three main clusters—Cluster 1, Cluster 2, and Cluster 3 (Fig. 7a). The preliminary findings suggest that the hinge region between the transmembrane domain and the soluble

https://doi.org/10.1038/s41467-024-54607-1

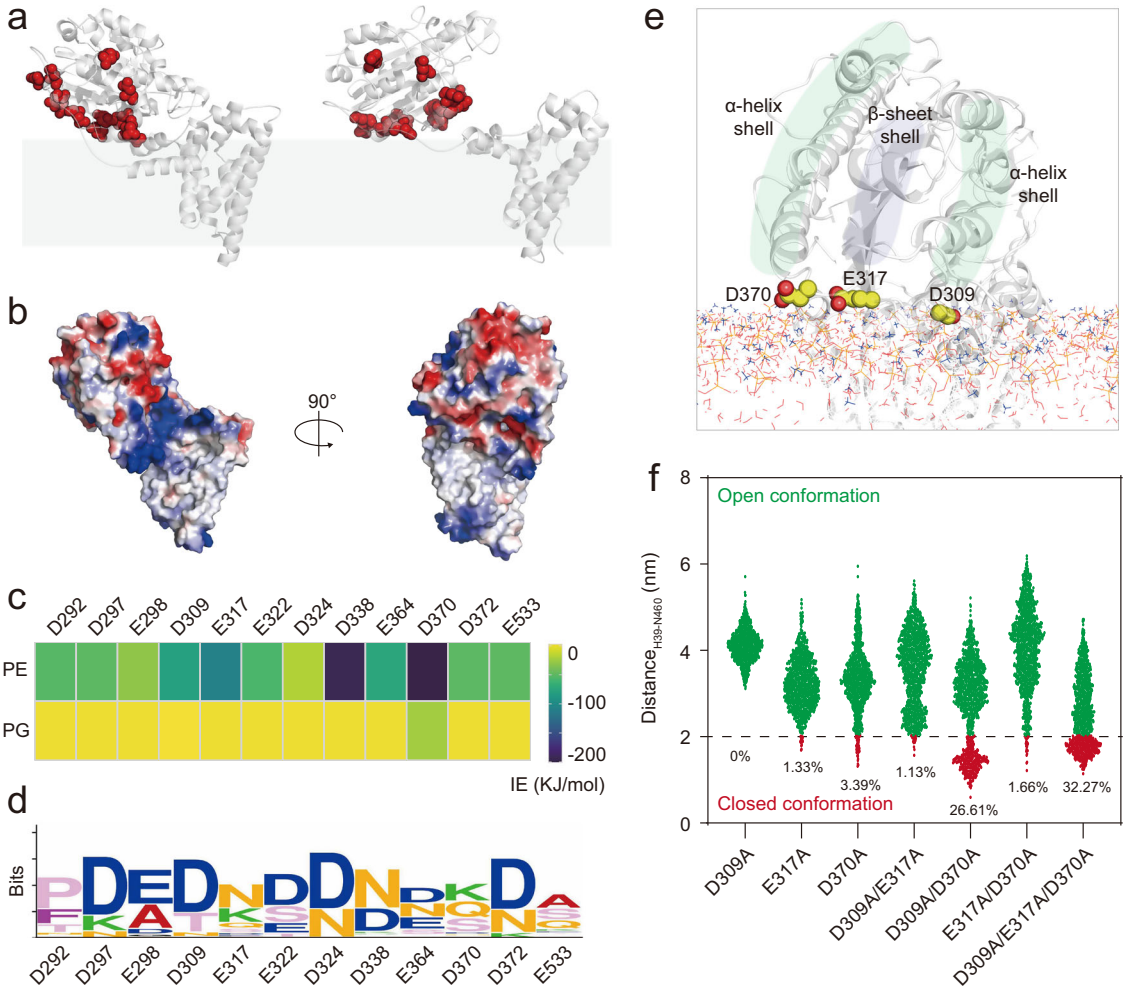

Fig. 4 | Interaction between EptA and the membrane regulates the stability of the EptA open conformation. a Spatial positions of acidic residues (red spheres) on the dorsal region of EptA soluble domain in the closed (left) and open (right) conformations. **b** Surface potentials of EptA, shown from both front and side views. Red surface indicates negative potential; blue surface indicates positive potential. **c** Interaction energy between acidic residues and PE and PG in the cell membrane. Data are shown as means. Source data are provided as a Source Data file. **d** Sequence profile of 7308 EptA protein sequences indicates the evolutionary conservation of the acidic residues involved in interactions with PE. **e** Spatial locations of residues D309, E317, and D370, subjected to computational mutational analysis. **f** Conformational distribution of EptA mutants calculated based on three simulation replicates. Source data are provided as a Source Data file.

domain of EptA, as well as the dorsal region of the soluble domain, play a pivotal role in regulating the conformational transition. We hypothesized that EptA sequences from different evolutionary branches might exhibit distinct sequence characteristics. Consequently, we analyzed the amino acid evolution in these two key regions across the three EptA clusters (Fig. 7b, c). Significant differences in the amino acid sequence motifs within the hinge region and the dorsal region of the soluble domain were observed among the three clusters. In Cluster 1, the hinge region motifs showed weak conservation, and the motifs in the dorsal region of the soluble domain were also weakly conserved, with acidic residues such as D and E appearing at only four sites. In Cluster 2, the hinge region motifs were the most strongly conserved, and acidic residues such as D and E were prevalent in the majority of the motifs in the dorsal region, though still weakly conserved. In Cluster 3, while the hinge region motifs were conserved, key interaction residues R117, R209, and E389 were mutated, preventing the formation of strong electrostatic interactions. The motifs in the dorsal region appeared at most sites and were more strongly conserved (Fig. 7b, c). These variations in amino acid motifs are likely to influence interactions both within the domains and between the soluble domain and the cell membrane. Based on the evolutionary analysis results, we propose that the EptA hinge region in Cluster 3 has the weakest electrostatic interactions, making it more prone to adopting an open conformation. Simultaneously, the soluble domains of EptA in Cluster 3 form the strongest interactions with the cell membrane, thereby enhancing the stability of the open conformation.

To test our hypothesis, we conducted molecular dynamics studies on EptA from *Helicobacter pylori* (*Hp*, Cluster 1) and *Salmonella enterica* (*Se*, Cluster 3), in addition to the EptA derived from *Neisseria meningitidis* (*Nm*, Cluster 2) used in the above analysis (Fig. S7). We examined the effect of EptA proteins from different species on the properties of the lipid membrane and found that they did not affect local lipid fluidity but slightly altered the curvature of the lipid around EptA, causing the upper leaflet to become concave and the lower leaflet to become convex (Fig. S8), consistent with findings in the literature[20]. This indicates that EptA may make complicated interactions with its surrounding membrane lipids. The three EptA variants displayed distinct conformational dynamics in the bacterial cell membrane environment (Fig. 7d). As noted previously, *Nm*EptA transitioned from a closed to an open conformation, while *Hp*EptA only exhibited a weak tendency to adopt the open conformation. In contrast, *Se*EptA could form a more extended conformation than *Nm*EptA.

We further analyzed the interaction energies of the hinge region between the transmembrane domains and soluble domains in the

https://doi.org/10.1038/s41467-024-54607-1

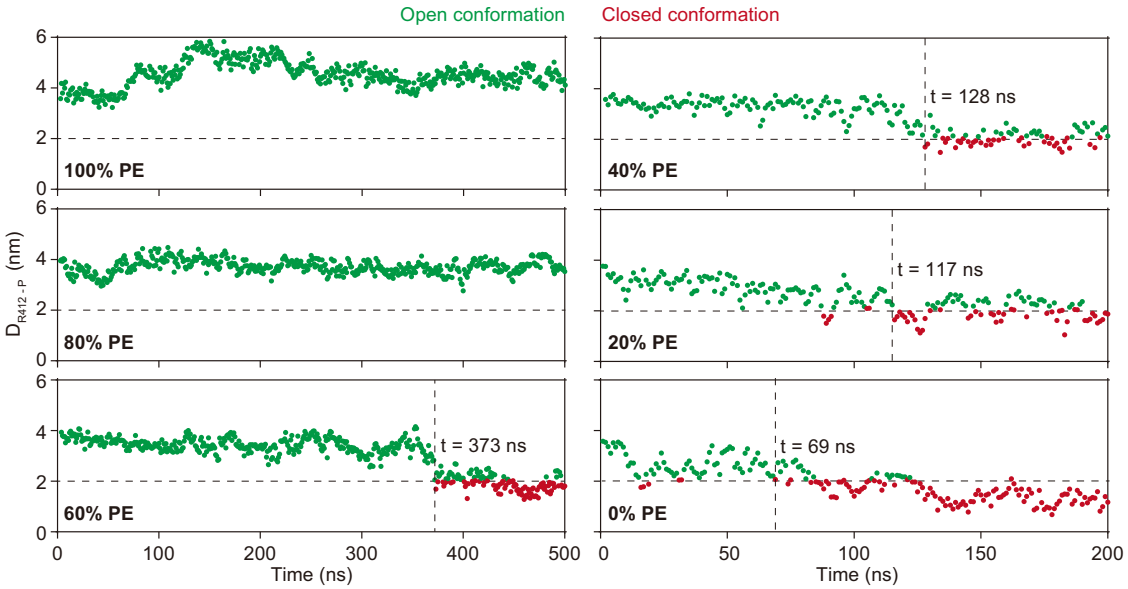

Fig. 5 | Conformational dynamics of EptA in membranes with various proportions of PE. A distance less than 2 nm is used as a cutoff to signify the closed conformation. Source data are provided as a Source Data file.

three EptAs. The interaction energies of the hinge regions were −542.7 kJ/mol for *Hp*EptA, −762.6 kJ/mol for *Nm*EptA, and −209.5 kJ/mol for *Se*EptA (Fig. 7e), with a stronger energy value indicating a potentially greater energy barrier to overcome when transitioning to an open state. Additionally, we examined the interaction energies of the three EptA soluble domains with the cell membrane, revealing values of −510.2 kJ/mol for *Hp*EptA, −1090.0 kJ/mol for *Nm*EptA, and −1211.4 kJ/mol for *Se*EptA (Fig. 7f). Stronger interaction energies not only facilitate the opening of soluble domains toward the cell membrane but also influence the stabilization of the open conformation. We calculated the free energies for the conformational transition of EptA from three different species in their PE-bound states. Specifically, the free energy barriers were 12.6 kcal/mol for *Hp*EptA, 4.3 kcal/mol for *Nm*EptA, and 3.3 kcal/mol for *Se*EptA (Fig. S9). These findings support their dynamic behaviors in unbiased classical simulations. Overall, these results suggest that the propensity for conformational transitions follows the order *Se*EptA>*Nm*EptA>*Hp*EptA, consistent with the observations from the molecular simulations (Fig. 7d). Furthermore, the conformational transitions of the three EptA proteins were reproduced across simulation replicates, indicating the reliability of the simulations (Fig. S10).

Through random sampling of amino acid residues in *Se*EptA, we investigated the distribution of electrostatic interactions within the protein (Fig. S11a). The results showed that the number of electrostatic interaction pairs averaged approximately 4.6 in the random sampling groups, while it was approximately 2 in the hinge region of *Se*EptA. This indicates that electrostatic interactions are weaker in the hinge region of *Se*EptA. We also analyzed the number of electrostatic interaction pairs in the hinge regions of all EptA proteins (86 in total) from Cluster 1 (*Hp*EptA), Cluster 2 (*Nm*EptA), and Cluster 3 (*Se*EptA). The average numbers were approximately 2.8, 4.0, and 2.4 pairs in three clusters, respectively (Fig. S11b). Additionally, we calculated the number of acidic residues in the dorsal region of the soluble domain of EptA proteins from three clusters, identifying averages of 14.5, 17.2, and 17.4 acidic residues, respectively (Fig. S11c). Our simulations revealed that fewer electrostatic pairs in the hinge region and more acidic residues in the dorsal region collectively contributed to the conformational transition of EptA. These findings explain why *Se*EptA is more prone to forming the open conformation.

Furthermore, we performed virtual mutagenesis on *Nm*EptA and *Se*EptA by exchanging their interfacial electrostatic residues. Specifically, we constructed the mutant R117A/E389N for *Nm*EptA and A118R/N389E for *Se*EptA. We performed MD simulations (with three replicates) for these two mutants and found that the R117A/E389N mutation in *Nm*EptA enhanced its conformational opening, similar to the dynamic behavior of the wild-type *Se*EptA. Meanwhile, the A118R/N389E mutation in *Se*EptA attenuated its conformational opening (Fig. S12). We calculated the free energy for the conformational transition of *Nm*EptA upon the mutation of R117A/E389N. We found that the free energy barrier reduced from 4.3 kcal/mol to 2.1 kcal/mol (Fig. S13). These results highlight the role of the electrostatic residues in modulating the conformational transition of EptA.

Discussion

In recent years, the emergence of MDR Gram-negative bacteria has posed a significant global challenge in the field of medicine[21,22]. The outer membrane of these bacteria acts as a crucial protective barrier against the external environment[5]. Within this membrane, LPS molecules undergo various modifications that enhance the barrier function and confer robust antibiotic resistance[23]. EptA, a prominent LPS-modifying enzyme in Gram-negative bacteria, plays a pivotal role in bacterial drug resistance by catalyzing LPS pEtN modification[24]. Previous studies have shown that EptA activity is tightly regulated and involves conformational transitions during catalysis[14,16,18]. However, the specific regulatory mechanisms governing these conformational transitions have never been reported.

The simulation results presented in this study reveal that the dorsal and ventral sides of the EptA soluble domain interact with the cell membrane surface and the transmembrane domain, respectively. The formation and disruption of these interactions are key factors influencing the observed conformational changes in EptA. This dynamic interplay allows EptA to bind PE and Re LPS in a coordinated manner, enabling regulation of its activity by the lipid nanoenvironment. EptA-mediated LPS modifications are a critical mechanism of antibiotic resistance in Gram-negative bacteria[15]. Therefore, inhibitors targeting EptA are being developed as effective antibiotic adjuvants to combat multidrug-resistant Gram-negative pathogens[25,26]. Our simulation results provide insights into the conformational

https://doi.org/10.1038/s41467-024-54607-1

a

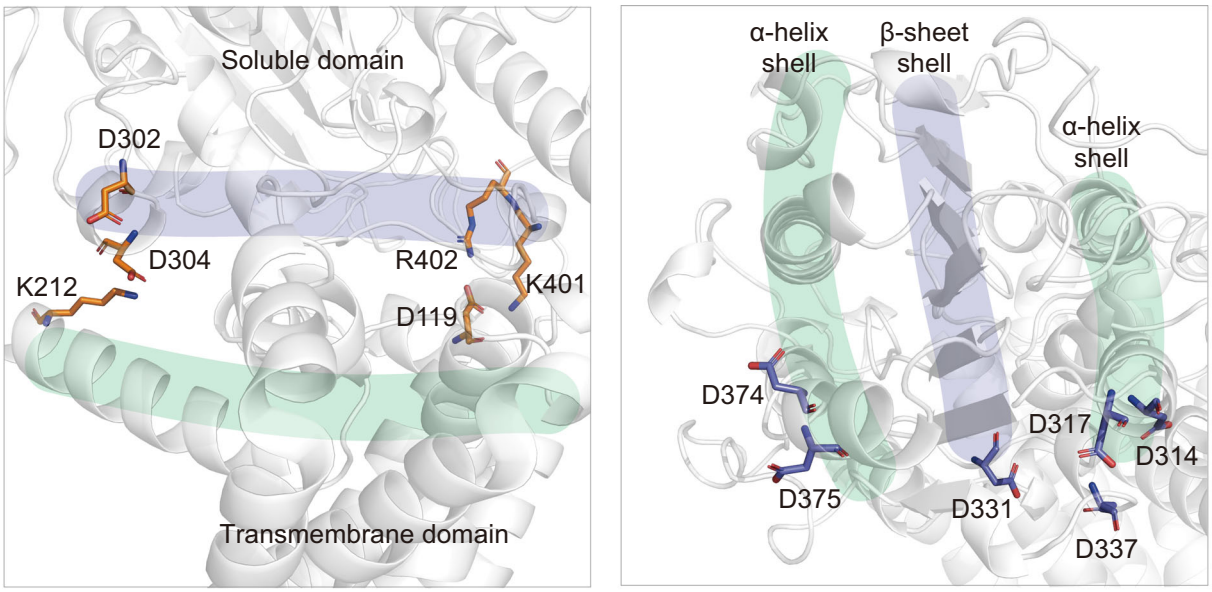

b

Minimum inhibitory concentrations against *E. coli* strains

Strains	MIC (mg/L)
(1) E. coli DH5α	<0.125 - 0.25
(2) *E. coli* DH5α-pUC19	<0.125
(3) *E. coli* DH5α-pUC19*mcr-1*	4
(4) *E. coli* DH5α-pUC19*mcr-1*-D302A/D304A	4
(5) *E. coli* DH5α-pUC19*mcr-1*-K401A/R402A	<0.125 - 0.25
(6) *E. coli* DH5α-pUC19*mcr-1*-D302A/D304A/K401A/R402A	0.25
(7) *E. coli* DH5α-pUC19*mcr-1*-D314A	4
(8) *E. coli* DH5α-pUC19*mcr-1*-D314A/D317A	4
(9) *E. coli* DH5α-pUC19*mcr-1*-D314A/D317A/D331A	2
(10) *E. coli* DH5α-pUC19*mcr-1*-D314A/D317A/D331A/D337A	1-2
(11) *E. coli* DH5α-pUC19*mcr-1*-D314A/D317A/D331A/D337A/D374A	<0.125
(12) *E. coli* DH5α-pUC19*mcr-1*-D314A/D317A/D331A/D337A/D374A/D375A	<0.125

Fig. 6 | Experimental mutations of key residues affect the function of MCR-1. a Electrostatic residues in the hinge region and acidic residues in the dorsal region of the soluble domain. **b** Minimum inhibitory concentrations of colistin against *E. coli* DH5α strains expressing wild-type and MCR-1 mutants.

landscape of EptA and identify its LPS binding pocket, offering a distinct binding site for the design of EptA-targeting inhibitors.

Earlier investigations proposed that the catalytic process of EptA follows a "ping-pong mechanism," where the PE donor first enters the protein's active center. After PE departs, EptA then binds to the Re LPS molecule, which acts as the acceptor[14,18]. The open conformation of EptA has been reported as necessary for binding larger Re LPS substrates, but the specific details of Re LPS binding remain unexplored[14]. Our study revealed that the previously hypothesized binding pocket PH2-PH2′ is insufficient for Re LPS binding. Instead, Re LPS binds within

https://doi.org/10.1038/s41467-024-54607-1

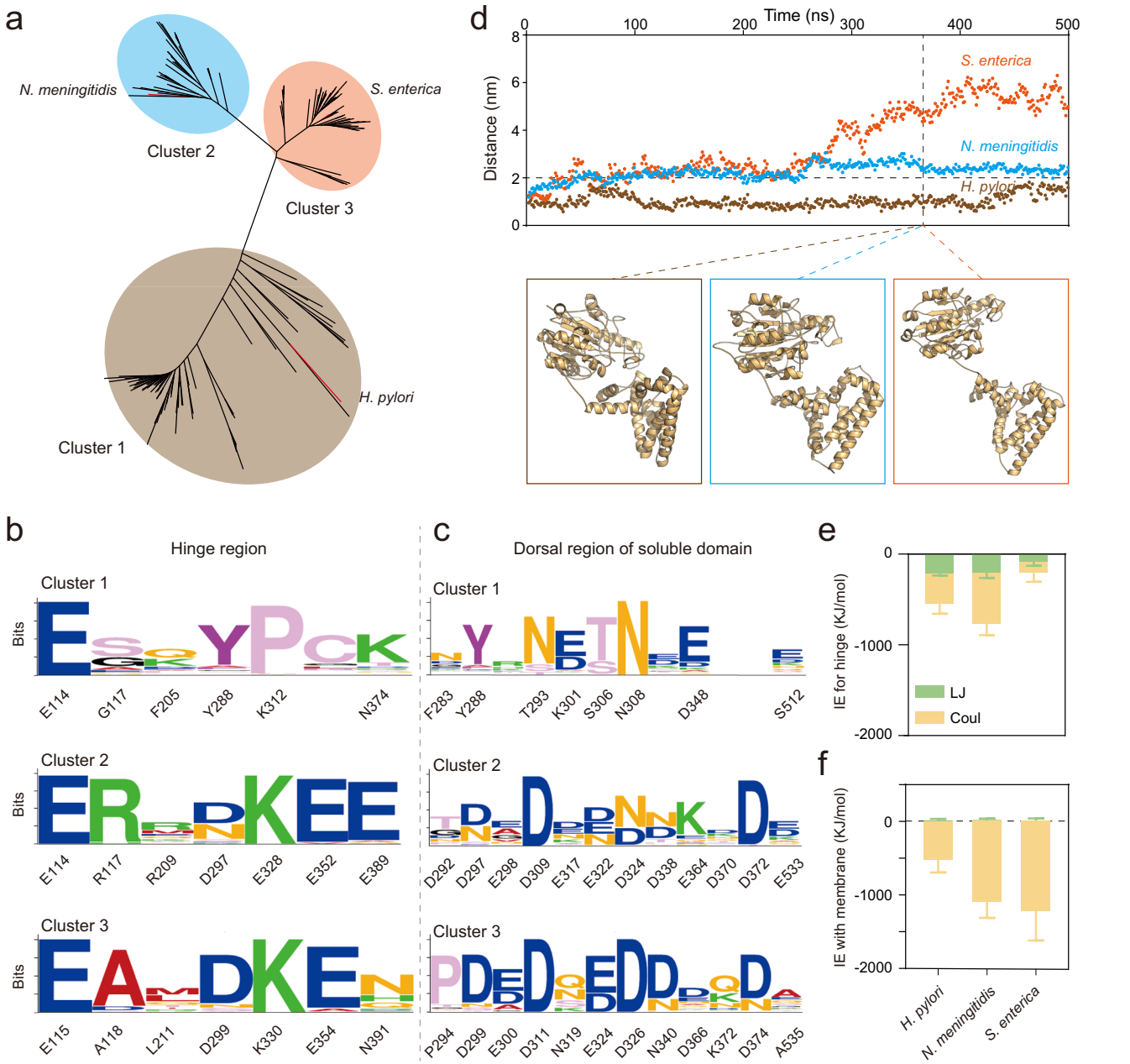

Fig. 7 | Different EptA proteins demonstrate a consistent conformational regulatory mechanism. a An unrooted evolutionary tree for the protein sequences of EptA from 160 species, Specifically, *Hp*EptA, *Nm*EptA, and *Se*EptA belong to Cluster 1 (brown), Cluster 2 (blue), and Cluster 3 (orange), respectively. **b** Sequence profiles of the residues in the EptA hinge region for the three clusters. **c** Sequence profiles of the residues in the EptA dorsal region of the soluble domain for three clusters. **d** Conformational dynamics of EptA from *Hp*EptA, *Nm*EptA, and *Se*EptA in the simulations. Source data are provided as a Source Data file. **e** Interaction energy of within the hinge regions of *Hp*EptA, *Nm*EptA, and *Se*EptA. Hydrophobic interactions are shown in green, while polar interactions are shown in yellow (n = 2001 independent estimations; data are presented as mean values ± SD). Source data are provided as a Source Data file. **f** Interaction energy between the membrane and the soluble domains of *Hp*EptA, *Nm*EptA, and *Se*EptA (n = 5001 independent estimations; data are presented as mean values ± SD). Source data are provided as a Source Data file.

the gap formed by the opening of the two domains, situated behind PH2-PH2′. Notably, the EptA homologous protein PbgA (YejM) exhibits a similar LPS-binding site, aligning with previous structural comparisons based on transmembrane domains (Fig. S14)[27,28].

Previous studies have occasionally observed PE substrates entering the active center between PH2-PH2′ and forming EptA-PEA intermediates[14,29,30]. However, these studies did not clarify why EptA-PEA intermediates can adopt an open conformation for binding Re LPS. Building upon this, our investigation reveals that once PE enters the active center, it competitively binds to interfacial residues. This binding disrupts the original interaction energy barrier between the two domains, promoting the formation of an open conformation. Subsequently, EptA can bind to the next substrate, Re LPS, ensuring sequential substrate binding and fulfilling the requirements of the "ping-pong mechanism". Moreover, experimental results indicate that the RodA-PBP2 complex regulates its activity through conformational changes between its transmembrane and soluble portions, akin to those observed in EptA[31]. Within this complex, mutations interfering with the contact between the transmembrane-soluble protein interface significantly increase the frequency of structural opening. This

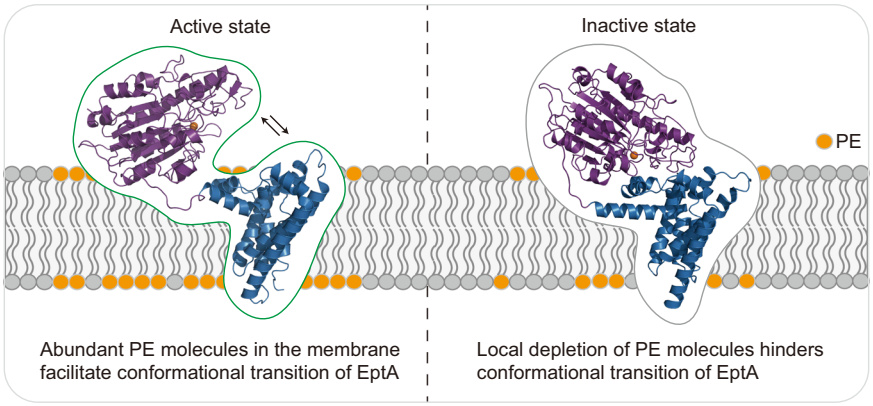

Fig. 8 | A schematic illustrating the relationship between the conformational transition of EptA and the lipid microenvironment in the membrane. The conformational transition of EptA is modulated by its local membrane environment, especially the abundance of PE. The head groups of PE molecules are highlighted in yellow.

suggests that regulating membrane protein function by manipulating the interface between the transmembrane and soluble portions may be a common mechanism in nature.

Recently, extensive research has focused on understanding how the nano-environment of the cell membrane, including factors like membrane thickness and fluidity, regulates membrane proteins[32]. Our findings demonstrate that the electrostatic properties of membrane surfaces can also finely regulate the function of membrane proteins. Previous simulations have assumed that positively charged residues dispersed on the surface of the soluble domain of EptA play a crucial role in their transition to and binding to the membrane surface[14]. This assumption stems from the common belief that, since phospholipid molecules are predominantly negatively charged, the cell membrane should interact with the positively charged region on the surface of membrane proteins[32]. Through regulating the PE molar content in the membrane environment and designing mutants with acidic amino acids on the membrane-bound surface, our study demonstrated that electrostatic interactions between the negatively charged residues of the soluble domain of EptA and the positively charged ethanolamine head group of PE in the cell membrane are the primary driving force for maintaining open conformational stability. The stronger the interaction between the PE molecule and the acidic residues of EptA, the longer its open conformation lasts and the greater the chance of binding to Re LPS. Notably, PE molecules play a dual role, acting as both substrates and activity regulators in EptA-catalyzed reactions. The depletion of PE molecules by EptA leads to a direct reduction in the proportion of PE in the cell membrane, subsequently diminishing the stability of the open conformation and ultimately inhibiting catalytic activity.

Experimental evidence indicates that certain fatty acid synthesis inhibitors can restrict phospholipid synthesis, leading to alterations in membrane lipid composition and ultimately impeding LPS modification in the outer membrane. This aligns with our findings, suggesting that modifying the nano-environment of the cell membrane can restore the sensitivity of drug-resistant bacteria to membrane-active antibiotics such as the polymyxins[33]. This contrasts with previous studies on the functional regulation of membrane proteins, where membrane lipids typically serve as functional regulators unaffected by protein function[32]. However, in the present case, PE is not only a functional regulator but also a substrate of the EptA-catalyzed reaction. The changes in the lipid environment regulating EptA's catalytic activity are induced by EptA itself. Consequently, we proposed a self-promoted model in which the conformational transition and catalytic activation of EptA was regulated by membrane lipid homeostasis, particularly the local content of PE (Fig. 8). This catalytic mechanism prevents EptA from initiating the catalytic cycle when the concentration of PE molecules is insufficient, avoiding excessive depletion of PE molecules—the primary component of phospholipids in the cell membrane.

In conclusion, our study elucidates the regulatory mechanism of outer membrane modification by EptA in Gram-negative bacteria and presents a paradigmatic illustration of how the lipid nano-environment of cell membranes influences and regulates the conformation of membrane proteins, thereby influencing their function. In response to the tightly regulated activity of the EptA enzyme, we propose a self-promoted model to explain its catalytic regulatory mechanism from the perspective of protein-lipid interactions. This model provides insights into maintaining a delicate balance between bacterial drug resistance and survival, offering a theoretical foundation for addressing EptA-mediated drug resistance in MDR Gram-negative bacteria.

Methods

System preparation

The protein structures utilized in this study were sourced from the Protein Data Bank Database (www.rcsb.org)[34] and AlphaFold Protein Structure Database (https://alphafold.com)[35]. The crystal structure of EptA from *N. meningitidis* (PDB: 5FGN) was determined through X-ray diffraction techniques, achieving a resolution of 2.75 Å[14]. Additionally, EptA proteins from *H. pylori* (UniProt: A0A438YQB9) and *S. enterica* (UniProt: A0A753AC37) were obtained from the AlphaFold Protein Structure Database (Fig. S7). The missing portions and the mutation of EptA were generated using the CHARMM-GUI PDB Reader & Manipulator[36].

The input files necessary for conducting MD simulations of the membrane protein complex were developed using the CHARMM-GUI membrane builder[37]. We determined the dominant acyl chain lengths of phospholipid in the membranes of *N. meningitidis*, *H. pylori*, and *S. enterica* through a comprehensive literature review (Table S2)[14,38–43]. The lipid compositions in the membrane components are provided in the Supplementary Information (Tables S2, S3 and S4). The structure of Re LPS from *N. meningitidis* was used to study its interaction with *Nm*EptA[44]. The membrane protein complex was situated within a simulation box with dimensions of $15 \times 15 \times 13\ nm^3$. Bilayers were built around the transmembrane regions of the protein by randomly placing lipids with the protein at the center of the x–y plane. An idealized surface area per lipid was utilized to ensure similar surface areas between the outer and inner leaflets of the membrane[45]. Following lipid placement, TIP3P water molecules were added to the system. Subsequently, an additional 0.1 M NaCl was introduced to neutralize the system and maintain physiological salt conditions. For simulations involving Re LPS within the membrane, 0.1 M $CaCl_2$ was also included to accurately mimic the biological context.

All-atom MD simulations for conformational sampling

To probe the dynamic behavior of EptA within the cell membrane, a series of conformational acquisition systems for EptA on the DPPE membrane were implemented. For EptA from *N. meningitidis*, two distinct systems were established: one with PE in the active center and another without. This design aimed to explore the influence of the PE substrate on the behavior of EptA. To delve into the distinctive features of EptA derived from different sources, the MD simulations were performed on EptA obtained from *H. pylori* and *S. enterica*. These simulations included the presence of the substrate PE within the active center of the proteins. To probe the stability of the open conformation, we simulated the open conformation of EptA (*N. meningitidis* and *S. enterica*) on the DPPE membrane. Simulation details of each system are shown in Table S2.

All-atom MD simulations for exploring the effects of PE gradients

To explore the dynamic behavior of EptA within various cell membrane compositions, PE gradient phospholipid bilayers were constructed for simulation. These bilayers were created with different ratios of DPPE to DLPG, specifically ratios of 10:0, 8:2, 6:4, 4:6, 2:8, and 0:10. EptA (open conformation) was placed onto these various phospholipid bilayer ratios to observe their closing behavior. Simulations were performed three times for the 0:10 ratio and twice for the 4:6 and 2:8 ratios. Systems with the 10:0, 8:2, and 6:4 ratios were each simulated for 500 ns, while systems with the 4:6, 2:8, and 0:10 ratios were simulated for 200 ns each. Simulation details of each system were shown in Table S3.

All-atom MD simulations for computational mutations

To explore the roles of the electrostatic residues in the hinge region and the acidic residues in the dorsal region of the soluble domain, a series of simulation systems were developed in which different EptA mutants were employed. All mutations of EptA were constructed in the CHARMM-GUI server[36]. Five-hundred nanosecond production simulations were conducted for each system with three replicates. Simulation details of each system were shown in Table S4.

Steered MD simulation, umbrella sampling, and free energy calculation

Steered simulations are widely used as an enhanced sampling approach in the research of biomolecular systems[46–48]. We employed this method to build the conformational transition pathway of EptA from its closed to open states. To enable the smooth transition of EptA, a harmonic potential was applied between the transmembrane and soluble domains. The initial force constant of the potential was set to 1000 kJ/mol/nm, and the pulling velocity was set to 0.025 nm/ns. The other simulation parameters were consistent with the unbiased MD simulation system. Umbrella sampling simulations were performed to elucidate the thermodynamics governing the conformational transition of EptA. Snapshots from the steered MD simulations were generated and used to initiate over 20 simulation windows in which the hinge region between the structural domains of EptA was restrained at fixed positions with a 0.1-nm interval. A 1000 kJ/mol/nm force constant of harmonic potential was used in umbrella sampling simulations. Each window was simulated for 50 ns to enhance conformational sampling, and the last 30-ns trajectories of each window were used to calculate a single free energy profile through the Weighted Histogram Analysis Method (WHAM)[49].

MD simulation parameters

Simulations were conducted using GROMACS 2019.5 with the CHARMM36m all-atom force field[50,51]. Energy minimizations were performed using the steepest descent method with a maximum force tolerance of 1000 kJ/mol/nm. To fully equilibrate the simulation system, six equilibration cycles were carried out by gradually turning off the position restraints on the lipids. Periodic boundary conditions were considered. All production simulations were conducted at constant temperature and pressure (NPT ensemble) which were maintained at 313.15 K using the Nose–Hoover algorithm and 1 bar using the semi-isotropic pressure coupling method with Parrinello–Rhaman barostat[52–54]. Electrostatic and Van der Waals interactions were calculated using the particle mesh Ewald method and Lennard–Jones potential algorithm, respectively[55]. The time step in production simulations was 2 fs. During equilibration, various positional and dihedral restraint potentials were applied and their force constants gradually reduced. No restraint potential was used for production simulations (with three replicates).

Bioinformatics analysis

To perform the phylogenetic analysis, 7308 EptA protein sequences from RefSeq database were aligned by MAFFT, with the Phylip format[56,57]. Additionally, 160 EptA protein sequences from UniPort database were aligned by MEGA11 software with the ClustalW algorithm utilizing default parameters, followed by a maximum-likelihood (ML) phylogenetic analysis using IQ-TREE version 2.2.2.6 (ultrafast bootstraps number, 1000)[58–60]. The WebLogo server was used to construct the sequence profiles of selected residue positions[61]. The interfacial residues between the two EptA domains were identified using Chimera, employing a cutoff distance of 5 Å (Table S5)[62]. The visualization of the simulation system and the analysis of protein potential vacuum electrostatics were performed using PyMOL[63]. The number of electrostatic interaction pairs and acidic residues in EptA were analyzed using an in-house Biopython-based Python script[64]. For the number of electrostatic interaction pairs, the protein was randomly divided into two intact protein regions, producing a series of random interfaces. The residue pair of D/E-R/K on either side of the interface was defined as an electrostatic interaction pair only when their distances were lower than 4 Å. For the number of acidic residues, the residues D/E on the dorsal region of the soluble domain were identified if their residue depth were smaller than 3.0 Å.

Simulation analysis

Most biophysical properties were analyzed using the internal tools in GROMACS. Names of the tools are listed in the brackets after the corresponding parameters. The interaction energy (*gmx energy*) between the active center residues and substrates (PE and Re LPS), as well as the interaction energy between the acidic residues and the membrane, were calculated[65,66]. The number of hydrogen bonds between PE and the interfacial regions of the transmembrane and soluble domains of EptA were calculated. In the present study, a hydrogen bond (*gmx hbond*) was considered to be formed if the acceptor–donor distance was less than 0.35 nm and the acceptor–hydrogen–donor angle was less than 30°[67]. The distances (*gmx mindist*) between the amino acid residues of EptA (H39, N460 in the *Nm*EptA; K40 and E443 in *Hp*EptA; L40 and N463 in *Se*EptA) and between the amino acid residue R412 and the phosphate atoms of the membrane were used to quantitatively analyze the opening and closing behaviors of EptA (Fig. S15). After removing the overall translational and rotational motions by superimposing the Cα atoms of each snapshot structure onto the starting structure using least-squares fitting, the RMSD (*gmx rms*) was calculated to analyze the structural stability of windows in umbrella sampling simulations[68]. The RMSD of each window in umbrella sampling indicates a stable sampling system (Fig. S16). The MDAnalysis program was used to analyze the effect of EptA on the membrane properties[69].

MCR-1 site-directed mutagenesis and MIC measurement

The *mcr-1* was amplified from a native *mcr-1* plasmid pHNSHP45 by PCR with primers XbaI_*mcr-1*_Fw and EcoRI_*mcr-1*_Rv (Table S6)[70]. Vector pUC19 and the amplified *mcr-1* were digested with XbaI and EcoRI, then purified using the Wizard® SV Gel and PCR Clean-Up System (Promega). The digested vector and *mcr-1* were ligated by incubating at 16 °C overnight, followed by transformation into chemical-competent *E. coli* DH5α. Successful transformants were selected on Luria-Bertani agar containing 100 mg/L ampicillin and further confirmed by Sanger sequencing using primers M13/pUC Reverse and M13/pUC Forward (Table S6). The mutation residues targeted in MCR-1 were selected based on the sequence and structural alignment between MCR-1 and *Nm*EptA. Site-directed mutagenesis was introduced using the Q5 Site-Directed Mutagenesis Kit (New England Biolabs) with the primers specified in Table S6. Sanger sequencing was conducted to validate the construction of mutants. The colistin MIC was determined using broth microdilution according to the European Committee on Antimicrobial Susceptibility Testing guidelines[71].

Reporting summary

Further information on research design is available in the Nature Portfolio Reporting Summary linked to this article.

Data availability

Previously published structure of *Nm*EptA from the PDB can be accessed via accession code 5FGN. The input and trajectories for MD simulations and the results from analysis software are available as a supplementary dataset on Zenodo (https://doi.org/10.5281/zenodo.13994576). Source data are provided with this paper.

Code availability

The program used for the analysis of protein structure is included in the code. All code is written using Python 3.7 and provided with this paper as a Supplementary Software file.

References

1. World Health Organization. Antimicrobial resistance: global report on surveillance. https://www.who.int/publications/i/item/9789241564748 (2014).
2. US Department of Health and Human Services. Antibiotic resistance threats in the United States 2019. https://www.cdc.gov/drugresistance/biggest-threats.html (2019).
3. Blair, J. M. A., Webber, M. A., Baylay, A. J., Ogbolu, D. O. & Piddock, L. J. V. Molecular mechanisms of antibiotic resistance. *Nat. Rev. Microbiol.* **13**, 42–51 (2015).
4. Needham, B. D. & Trent, M. S. Fortifying the barrier: the impact of lipid A remodelling on bacterial pathogenesis. *Nat. Rev. Microbiol.* **11**, 467–481 (2013).
5. Rojas, E. R. et al. The outer membrane is an essential load-bearing element in Gram-negative bacteria. *Nature* **559**, 617–621 (2018).
6. Raetz, C. R. H., Reynolds, C. M., Trent, M. S. & Bishop, R. E. Lipid A modification systems in Gram-negative bacteria. *Annu. Rev. Biochem.* **76**, 295–329 (2007).
7. Sue, C. N., Mohammad, A. K. A., Tony, V., Qi, Z. & Jian, L. Rescuing the last-line polymyxins: achievements and challenges. *Pharmacol. Rev.* **73**, 679 (2021).
8. Freire, C., Taunay-Rodrigues, A., Gonzatti, M. B., Fonseca, F. M. P. & Freire, J. New insights about the EptA protein and its correlation with the pmrC gene in polymyxin resistance in Pseudomonas aeruginosa. *Curr. Res. Microb. Sci.* **2**, 100042 (2021).
9. Samantha, A. & Vrielink, A. Lipid A phosphoethanolamine transferase: regulation, structure and immune response. *J. Mol. Biol.* **432**, 5184–5196 (2020).
10. Stojanoski, V. et al. Structure of the catalytic domain of the colistin resistance enzyme MCR-1. *BMC Biol.* **14**, 81 (2016).
11. Sun, J., Zhang, H., Liu, Y.-H. & Feng, Y. Towards understanding MCR-like colistin resistance. *Trends Microbiol.* **26**, 794–808 (2018).
12. Wang, Y. et al. Comprehensive resistome analysis reveals the prevalence of NDM and MCR-1 in Chinese poultry production. *Nat. Microbiol.* **2**, 16260 (2017).
13. Feng, Y. Transferability of MCR-1/2 polymyxin resistance: complex dissemination and genetic mechanism. *ACS Infect. Dis.* **4**, 291–300 (2018).
14. Anandan, A. et al. Structure of a lipid A phosphoethanolamine transferase suggests how conformational changes govern substrate binding. *Proc. Natl. Acad. Sci. USA* **114**, 2218–2223 (2017).
15. Kahler, C. M., Nawrocki, K. L., Anandan, A., Vrielink, A. & Shafer,W. M.Structure-function relationships of the Neisserial EptA enzyme responsible for phosphoethanolamine decoration of lipid A: rationale for drug targeting. *Front. Microbiol.* **9**, 1922 (2018).
16. Yang, Q. et al. Balancing mcr-1 expression and bacterial survival is a delicate equilibrium between essential cellular defence mechanisms. *Nat. Commun.* **8**, 2054 (2017).
17. Zhu, Y. et al. Polymyxins bind to the cell surface of unculturable Acinetobacter baumannii and cause unique dependent resistance. *Adv. Sci.* **7**, 2000704 (2020).
18. Anandan, A. et al. Conformational flexibility of EptA driven by an interdomain helix provides insights for enzyme–substrate recognition. *IUCrJ* **8**, 732–746 (2021).
19. Xu, Y. et al. An evolutionarily conserved mechanism for intrinsic and transferable polymyxin resistance. *mBio* **9**, e02317–e02317 (2018).
20. Newport, T. D., Sansom, M. S. P. & Stansfeld, P. J. The MemProtMD database: a resource for membrane-embedded protein structures and their lipid interactions. *Nucleic Acids Res.* **47**, D390–D397 (2019).
21. Mills, J. P. & Marchaim, D. Multidrug-resistant Gram-negative bacteria: infection prevention and control update. *Infec. Dis. Clin. N. Am.* **35**, 969–994 (2021).
22. Murray, C. J. L. et al. Global burden of bacterial antimicrobial resistance in 2019: a systematic analysis. *Lancet* **399**, 629–655 (2022).
23. Simpson, B. W. & Trent, M. S. Pushing the envelope: LPS modifications and their consequences. *Nat. Rev. Microbiol.* **17**, 403–416 (2019).
24. Anandan, A. & Vrielink, A. Structure and function of lipid A–modifying enzymes. *Ann. N. Y. Acad. Sci.* **1459**, 19–37 (2020).
25. Harris, T. L. et al. Small molecule downregulation of PmrAB reverses lipid A modification and breaks colistin resistance. *ACS Chem. Biol.* **9**, 122–127 (2014).
26. Mullally, C. et al. Novel small molecules that increase the susceptibility of Neisseria gonorrhoeae to cationic antimicrobial peptides by inhibiting lipid A phosphoethanolamine transferase. *J. Antimicrob. Chemoth.* **77**, 2441–2447 (2022).
27. Clairfeuille, T. et al. Structure of the essential inner membrane lipopolysaccharide-PbgA complex. *Nature* **584**, 479–483 (2020).
28. Gabale, U., Peña Palomino, P. A., Kim, H., Chen, W. & Ressl, S. The essential inner membrane protein YejM is a metalloenzyme. *Sci. Rep.* **10**, 17794 (2020).
29. Sun, Z. & Palzkill, T. Deep mutational scanning reveals the active-site sequence requirements for the colistin antibiotic resistance enzyme MCR-1. *mBio* **12**, e0277621 (2021).
30. Wanty, C. et al. The Structure of the neisserial lipooligosaccharide phosphoethanolamine transferase A (LptA) required for resistance to polymyxin. *J. Mol. Biol.* **425**, 3389–3402 (2013).
31. Nygaard, R. et al. Structural basis of peptidoglycan synthesis by E. coli RodA-PBP2 complex. *Nat. Commun.* **14**, 5151 (2023).
32. Levental, I. & Lyman, E. Regulation of membrane protein structure and function by their lipid nano-environment. *Nat. Rev. Mol. Cell Biol.* **24**, 107–122 (2023).
33. Carfrae, L. A. et al. Inhibiting fatty acid synthesis overcomes colistin resistance. *Nat. Microbiol.* **8**, 1026–1038 (2023).

34. Burley, S. K. et al. RCSB protein data bank (RCSB.org): delivery of experimentally-determined PDB structures alongside one million computed structure models of proteins from artificial intelligence/machine learning. *Nucleic Acids Res.* **51**, D488–D508 (2023).
35. Varadi, M. et al. AlphaFold protein structure database: massively expanding the structural coverage of protein-sequence space with high-accuracy models. *Nucleic Acids Res.* **50**, D439–D444 (2021).
36. Park, S. J., Kern, N., Brown, T., Lee, J. & Im, W. CHARMM-GUI PDB Manipulator: various PDB structural modifications for biomolecular modeling and simulation. *J. Mol. Biol.* **435**, 167995 (2023).
37. Feng, S., Park, S., Choi, Y. K. & Im, W. CHARMM-GUI Membrane Builder: past, current, and future developments and applications. *J. Chem. Theory Comput.* **19**, 2161–2185 (2023).
38. Shimomura, H., Hosoda, K., Hayashi, S., Yokota, K. & Hirai, Y. Phosphatidylethanolamine of Helicobacter pylori functions as a steroid-binding lipid in the assimilation of free cholesterol and 3β-hydroxl steroids into the bacterial cell membrane. *J. Bacteriol.* **194**, 2658–2667 (2012).
39. Cho, Y.-T. et al. Differentiation of virulence of Helicobacter pylori by matrix-assisted laser desorption/ionization mass spectrometry and multivariate analyses. *Clin. Chim. Acta* **424**, 123–130 (2013).
40. Modak, M. J., Nair, S. & Venkataraman, A. Studies on the fatty acid composition of some Salmonellas. *J Gen Microbiol* **60**, 151–157 (1970).
41. Lagha, R., Ben Abdallah, F. & Masmoudi, A. S. Effect of combined long-term starvation and γ-irradiation on membrane fatty acids and cell surface hydrophobicity of Salmonella enterica serovar Typhimurium. *J. Dairy Sci.* **98**, 8525–8530 (2015).
42. Guo, L. et al. Lipid A acylation and bacterial resistance against vertebrate antimicrobial peptides. *Cell* **95**, 189–198 (1998).
43. Zhang, J. I. et al. Rapid direct lipid profiling of bacteria using desorption electrospray ionization mass spectrometry. *Int. J. Mass Spectrom.* **301**, 37–44 (2011).
44. Trent, M. S., Stead, C. M., Tran, A. X. & Hankins, J. V. Diversity of endotoxin and its impact on pathogenesis. *J. Endotoxin. Res.* **12**, 205–223 (2006).
45. Doktorova, M. & Weinstein, H. Accurate in silico modeling of asymmetric bilayers based on biophysical principles. *Biophys. J.* **115**, 1638–1643 (2018).
46. Célerse, F., Lagardère, L., Derat, E. & Piquemal, J.-P. Massively parallel implementation of steered molecular dynamics in tinker-HP: comparisons of polarizable and non-polarizable simulations of realistic systems. *J. Chem. Theory Comput.* **15**, 3694–3709 (2019).
47. Li, M., Bao, Y., Xu, R., La, H. & Guo, J. Critical extracellular Ca2+ dependence of the binding between PTH1R and a G-protein peptide revealed by MD simulations. *ACS Chem. Neurosci.* **13**, 1666–1674 (2022).
48. Kumar, N. & Garg, P. Probing the molecular basis of cofactor affinity and conformational dynamics of mycobacterium tuberculosis elongation factor tu: an integrated approach employing steered molecular dynamics and umbrella sampling simulations. *J. Phys. Chem. B* **126**, 1447–1461 (2022).
49. Hub, J. S., de Groot, B. L. & Van der Spoel, D. g_wham—a free weighted histogram analysis implementation including robust error and autocorrelation estimates. *J. Chem. Theory Comput.* **6**, 3713–3720 (2010).
50. Van Der Spoel, D. et al. GROMACS: fast, flexible, and free. *J. Comput. Chem.* **26**, 1701–1718 (2005).
51. Huang, J. et al. CHARMM36m: an improved force field for folded and intrinsically disordered proteins. *Nat. Methods* **14**, 71–73 (2017).
52. Hoover, W. G. Canonical dynamics: equilibrium phase-space distributions. *Phys. Rev. A* **31**, 1695–1697 (1985).
53. Nosé, S. A molecular dynamics method for simulations in the canonical ensemble. *Mol. Phys.* **52**, 255–268 (1984).
54. Parrinello, M. & Rahman, A. Polymorphic transitions in single crystals: a new molecular dynamics method. *J. Appl. Phys.* **52**, 7182–7190 (1981).
55. Darden, T., York, D. & Pedersen, L. Particle mesh Ewald: an N·log(N) method for Ewald sums in large systems. *J. Chem. Phys.* **98**, 10089–10092 (1993).
56. Nakamura, T., Yamada, K. D., Tomii, K. & Katoh, K. Parallelization of MAFFT for large-scale multiple sequence alignments. *Bioinformatics* **34**, 2490–2492 (2018).
57. O'Leary, N. A. et al. Reference sequence (RefSeq) database at NCBI: current status, taxonomic expansion, and functional annotation. *Nucleic Acids Res.* **44**, D733–D745 (2016).
58. Tamura, K., Stecher, G. & Kumar, S. MEGA11: molecular evolutionary genetics analysis version 11. *Mol. Biol. Evol.* **38**, 3022–3027 (2021).
59. Minh, B. Q. et al. IQ-TREE 2: new models and efficient methods for phylogenetic inference in the genomic era. *Mol. Biol. Evol.* **37**, 1530–1534 (2020).
60. The UniProt Consortium. UniProt: a worldwide hub of protein knowledge. *Nucleic Acids Res.* **47**, D506–D515 (2019).
61. Crooks, G. E., Hon, G., Chandonia, J.-M. & Brenner, S. E. J. G. r. WebLogo: a sequence logo generator. *Genome Res.* **14**, 1188–1190 (2004).
62. Pettersen, E. F. et al. UCSF Chimera—a visualization system for exploratory research and analysis. *J. Comput. Chem.* **25**, 1605–1612 (2004).
63. Yuan, S., Chan, H. C. S. & Hu, Z. Using PyMOL as a platform for computational drug design. *WIREs Comput. Mol. Sci.* **7**, e1298 (2017).
64. Cock, P. J. et al. Biopython: freely available Python tools for computational molecular biology and bioinformatics. *Bioinformatics* **25**, 1422–1423 (2009).
65. Cornell, W. D. et al. A second generation force field for the simulation of proteins, nucleic acids, and organic molecules. *J. Am. Chem. Soc.* **117**, 5179–5197 (1995).
66. Luty, B. A., Tironi, I. G. & Van Gunsteren, W. F. Lattice-sum methods for calculating electrostatic interactions in molecular simulations. *J. Chem. Phys.* **103**, 3014–3021 (1995).
67. Van der Spoel, D., Van Maaren, P. J., Larsson, P. & Tîmneanu, N. Thermodynamics of hydrogen bonding in hydrophilic and hydrophobic media. *J. Phys. Chem. B* **110**, 4393–4398 (2006).
68. Maiorov, V. N. & Crippen, G. M. Size-independent comparison of protein three-dimensional structures. *Proteins* **22**, 273–283 (1995).
69. Naughton, F. B. et al. MDAnalysis 2.0 and beyond: fast and interoperable, community driven simulation analysis. *Biophys. J.* **121**, 272a–273a (2022).
70. Liu, Y.-Y. et al. Emergence of plasmid-mediated colistin resistance mechanism MCR-1 in animals and human beings in China: a microbiological and molecular biological study. *Lancet. Infect. Dis.* **16**, 161–168 (2016).
71. The European Committee on Antimicrobial Susceptibility Testing. Breakpoint tables for interpretation of MICs and zone diameters.Version 14.0, https://www.eucast.org (2024).

Acknowledgements

We thank the HPC Cloud Team from Shandong University for their technical supports in the large-scale parallel computation. We thank Dr Phillip J. Bergen from Monash University for his suggestions in writing the manuscript. This work was partly supported by the National Key Research and Development Program of China 2023YFC3403502 (to X.J.), National Natural Science Foundation of China 32301041 (to X.J.), Shandong Excellent Young Scientists (Overseas) Fund Program 2023HWYQ-044 (to X.J.) and Natural Science Foundation of Shandong Province ZR2022QC014 (to X.J.).

Author contributions

Z.M., S.C.N., Z.L., J.Z., and K.M. performed and analyzed experiments. M.X., and L.W. offered computational resource. J.L., and X.J. conceived and wrote the paper with input from Z.M., and L.X.

Competing interests

The authors declare no competing interests.

Additional information

Supplementary information The online version contains supplementary material available at https://doi.org/10.1038/s41467-024-54607-1.

Correspondence and requests for materials should be addressed to Jian Li or Xukai Jiang.

Peer review information *Nature Communications* thanks Charlene Kahler, and the other, anonymous, reviewer(s) for their contribution to the peer review of this work. A peer review file is available.